

¹ Cover Letter

² **A Fast Method for Detecting Rock Blocks and Calculating Volumes and 3D Surface Areas**

³ Ali Polat

⁴ Dear Editors-in-Chief,

⁵
⁶ please find the enclosed manuscript "..." which we are submitting for exclusive consideration for publication in Com-
⁷ puters & Geosciences. We confirm that the submission follows all the requirements and includes all the items of the
⁸ submission checklist.

⁹
¹⁰ The manuscript presents ...

¹¹
¹² We provide the source codes in a public repository with details listed in the section "Code availability".

¹³
¹⁴ Thanks for your consideration.

¹⁵
¹⁶ Sincerely,

¹⁷
¹⁸ Authors names
¹⁹ Corresponding author affiliation and e-mail

²⁰
²¹ **Delete before submission:**

²² Please confirm that your submission follows all the requirements of the guidelines, including the submission checklist:

- ²³ - Cover letter
- ²⁴ - Highlights
- ²⁵ - Authorship statement
- ²⁶ - The manuscript must be single column and double spaced
- ²⁷ - Reference must be in the author-date format
- ²⁸ - Code availability section

²⁹ *The manuscripts that do not meet the requirement guidelines will be desk-rejected.

30 Highlights

31 **A Fast Method for Detecting Rock Blocks and Calculating Volumes and 3D Surface Areas**

32 Ali Polat

33 • Highlight 1

34 • Highlight 2

35 • Highlight 3

36 • Highlight 4

37 • Highlight 5

38 **A Fast Method for Detecting Rock Blocks and Calculating Volumes
39 and 3D Surface Areas**

40 **Ali Polat**

41 *Provincial Directorate of Disaster and Emergency, 58000, Sivas, Turkey*

42

43 **ARTICLE INFO**

44

45 *Keywords:*

46 Rock segmentation

47 U-Net

48 Convolutional Neural Networks

49 Rockfall

50 Volume Calculation

51 3D Surface Area Calculation

52

53

54

55

56

57

58

59

60

61

62

63

64

65 **ABSTRACT**

Rockfall events are a type of natural disaster that causes loss of life and property in the world. The risk of rockfall can be eliminated by using rockfall prevention methods. To choose the most suitable method, projecting studies should be carried out. This study aims to automatically detect rock blocks in a region and calculate their volumes and 3D surface areas. For this purpose, U-Net segmentation method and Python software language were used. DenseNet121 transfer learning method based on convolutional neural networks was used for feature extraction. The data set was created from the orthophoto image obtained by an unmanned aerial vehicle (UAV). Using the random sampling method, 369 images were selected for training and 191 images for testing. As a result of the analysis, the mean IOU (Intersection Over Union) was calculated as 85% for training and 84% for testing. The trained model was applied to the study area and 3111 rock blocks were detected. This file is saved with coordinates and can be open in any GIS software and its geometrical properties can be calculated. The volumes and 3D surface areas of the rock blocks were calculated with Python software as 275.93 m^3 and 2615.23 m^2 , respectively. With this study, rock blocks can be detected automatically, and their volumes and 3D surface areas can be measured. These results can be used in the selection of rockfall prevention methods. In addition, the codes used in this study can automatically detect different geological formations from aerial photographs. Also, volume and 3D surface area algorithms developed in this study can be used to calculate different types of objects.

65 **1. Introduction**

66 In many parts of the world, loss of life and property is experienced, and large-scale economic losses occur due to
67 natural disasters. One of these natural disasters is rockfall events. Rockfalls are a type of slope instability in which
68 blocks of rock confined to discontinuities move very rapidly from the source region (Varnes, 1978; Hutchinson, 1988;
69 Cruden and Varnes, 1996). Due to the high velocity during the event, rockfalls can be very dangerous for structures
70 in their route depending on the block size. Although it is a type of disaster that affects small areas, its consequences
71 can be very serious. That's why rockfall prevention studies are important. There are also studies on this subject in
72 the literature (Liu et al., 2021; Keskin and Polat, 2022; Ji et al., 2023; Kainthola et al., 2023; Cao et al., 2024). Some
73 preliminary studies are needed to develop a prevention method. One of them is the detection of rock blocks and the
74 calculation of their geometric properties. In this study, rock blocks were segmented, and their volumes and 3D surface
75 areas were calculated. There are various studies on rock segmentation in the literature.

76 In 2006, Dunlop (Dunlop, 2006) developed a technique for characterization of rocks using albedo, colour, tex-
77 ture and shape features. In that work rocks in natural scenes are segmented and located with an accurate boundary.
78 For segmentation purpose top-down and bottom-up knowledge are combined, and geologic rock analysis performed

ORCID(s): 0000-0002-9147-3633 (A. Polat)

79 successfully.

80 In the study carried out by Song (Song and Shan, 2006) in this area in 2006, segmentation studies of rocks on
81 Mars were carried out in order to plan the route and determine the landing areas. Texture-based image segmentation
82 and edge-flow driven active contour has been developed. Wavelet based local transform, multi-resolution histograms,
83 and inter-scale decision were combined and used for rock segmentation. As a result of the experiments, reliable rock
84 segmentation results were obtained by Song.

85 The place of visual navigation in planetary rover autonomy is crucial. Rock segmentation is an important and
86 challenging task for rover autonomy due to the high computational load and real-time requirement. Kuang et al.
87 (Kuang et al., 2021) propose a rock segmentation network (NI-U-Net++) to aid in the visual navigation of rovers. The
88 created model consists of two stages. In the first step, called pre-training, synthetic rock images are created and then
89 the generated images are used to pre-train the NI-U-Net++ network. The second phase, transfer-training, fine-tunes
90 the pre-trained NI-U-Net++ network with real-life images.

91 Guo et al. (Guo et al., 2022) proposed an adaptive watershed segmentation method based on distance transformation
92 for blasted rock piles images. They obtained 95.65% segmentation accuracy for limestone and granite rock blocks with
93 area over 100 cm².

94 Segmentation of rocks is important in mining as well as in geology. Segmentation is used in this area to deter-
95 mine the size distribution of rock fragments, to organize and optimize blasting, and to reduce environmental impact.
96 For this purpose, Malladi et al. (Malladi et al., 2014) proposed a simple superpixel algorithm called Superpixels Us-
97 ing Morphology (SUM), which uses a watershed transformation approach to generate superpixels; and made a study
98 comparing some of the current superpixel algorithms on rock images.

99 Recently, various deep learning and machine learning algorithms, including Convolutional Neural Networks (CNN),
100 have been proposed by researchers working on rock segmentation. Karimpouli and Tahmasebi (Karimpouli and Tah-
101 masebi, 2019) used convolutional autoencoder networks called SegNet for segmentation of digital rock images. Due to
102 the limited number of rock images, cross-correlation based simulation was applied to increase the number of images.
103 20 images taken from Berea sandstone were used as dataset. As a result of the tests, they obtained an accuracy value
104 of 96

105 Xue et al. (Xue et al., 2021) made rock segmentation study for a different purpose; they proposed the rock seg-
106 mentation visual system to assist Tunnel Boring Machine (TBM) driving. TBM is an essential equipment for digging
107 long-range tunnels. They applied different deep learning network for semantic segmentation of rocks.

108 In the above studies, rock segmentation was carried out for different purposes. In this study, rock segmentation
109 was carried out as a necessary preliminary study in the development of rockfall prevention methods. Rock blocks were
110 detected precisely in a fast, economical and safe way. In addition, the volumes and 3D surface areas of rock blocks were

¹¹¹ calculated. The methods and algorithms used in the study can be used in many fields such as engineering applications,
¹¹² and geological-geomorphological studies.

¹¹³ **1.1. Study area**

¹¹⁴ The study area is in the north of Karasar village, which is approximately 156 km away from Sivas city (Fig. 1).
¹¹⁵ This area consists of Middle Miocene aged agglomerate and tuff units (MTA 1/25000) (Fig. 2). This unit was defined
¹¹⁶ as Adatepe volcanites according to (Yilmaz and Yilmaz, 2004). The unit consists of black, red-brown, and brown-
¹¹⁷ black colored basaltic lava flows and less commonly agglomerate and tuffs. The rock blocks in this unit expose a risk
¹¹⁸ of rockfall. Lower Miocene aged sandstone-mudstone-limestone units are observed in the settlement area (Karasar
¹¹⁹ village) and vicinity.

¹²⁰ Karasar village is located on the slopes of a hill. The bedrock on the hill is heavily fractured and cracked. There
¹²¹ are many rock blocks that have fallen from the upper parts of the slope. The sizes of these blocks vary from $0.5 m^3$ to
¹²² $15 m^3$. Rapid temperature changes, heavy snow and precipitation, freeze-thaw, earthquake, and human-induced causes
¹²³ increase the risk of rockfall in the region.

¹²⁴ **2. Methodology**

¹²⁵ Creating the dataset is a big problem for classification or segmentation processes. In this study, Unmanned Air
¹²⁶ Vehicle (UAV) was used to collect data. An orthophoto image of the region was created from aerial photographs
¹²⁷ obtained by UAV. An area was selected to create train images. Rock blocks within this area were labelled and mask
¹²⁸ images were created. Then segmentation process was completed by Python and necessary libraries, and the results
¹²⁹ were converted to the polygon as a vector file (Fig. 3). Moreover, the volumes of all the rocks were calculated. This
¹³⁰ section includes an example of equation.

¹³¹ **2.1. Data preparation**

¹³² In this study required data was collected by UAV. DJI phantom 3-Pro was used for image acquisition. First, the
¹³³ area to be flown is determined, then the necessary parameters for image acquisition are entered by the Pix4d Capture
¹³⁴ software. These parameters were chosen as follows.

- ¹³⁵ – Flight altitude (altitude): 100 m.
- ¹³⁶ – Flight speed (speed): Fast
- ¹³⁷ – Camera angle (Angle): 70°
- ¹³⁸ – Overlap: 80%

¹³⁹
¹⁴⁰ The flight was carried out by the "Double Grid" method. The model of UAV used in this study does not have an

141 obstacle detecting feature. Therefore, when determining the height, it is necessary to pay attention to the nearby power
 142 lines, tall buildings, trees, and peaks of hills.

143 The camera model (FC00X) of UAV has 4000x3000 resolution, 3.61 mm focal length and 1.56 x 1.56 μm pixel
 144 dimensions. After the flight, 284 images were obtained, and these images were processed with the Pix4Dmapper
 145 software. As a result, an orthophoto image with a resolution of 3.51 cm/pixel and a dimension of 2329x1587 was
 146 created.

147 An area was selected to create train and test images from large orthophoto image. This area was selected randomly.
 148 Then all rocks seen on the image were drawn on by GIS software. This file was saved as a vector file, and it will be
 149 used as mask data in segmentation processes. After this process, we have created the image and mask files. A deep
 150 learning model requires the same sizes of images. That's why a single image needs to be split into patches. The patch
 151 dimension was used as 256x256. Train-test splitting size was selected as 66% for training data and 34% for testing
 152 data. The large image was split into 9 part to avoid sampling from the same regions. Areas 1,5,9 were selected for
 153 creating test images. Train images were selected from the others (2,3,4,6,7,8) areas (Fig. 4). A total of 600 images
 154 (256x256) were selected, 369 images for training and 191 images for testing. The same processes were applied to
 155 extract the mask images.

156 We also used the Albumentations (Buslaev et al., 2020) method for data augmentation during the model-building
 157 stage. Albumentations includes many transform methods. We applied augmentation methods given below:

- 158 – horizontal flip
- 159 – affine transforms
- 160 – perspective transforms
- 161 – brightness/contrast/colours manipulations
- 162 – image blurring and sharpening
- 163 – gaussian noise

164

165 2.2. Model building

166 In this study, U-Net architecture (Ronneberger et al., 2015) was used as a segmentation model. This architecture
 167 is a type of fully convolutional network developed for biomedical image segmentation. It is named U-Net because the
 168 shape of the architecture is like the letter U. The network architecture of U-Net is shown in Figure 5. It consists of two
 169 parts. These are the contracting path (left side) and expanding path (right side). The first part captures context, and the
 170 second part enables precise localization. The left side consists of 4 blocks and each block contains two 3x3 convolution
 171 layers + activation function (with batch normalization) and one 2x2 max-pooling layer. Also, the right side consists of

172 4 blocks. These blocks include the steps of deconvolution layer, merging with feature map from subsampling path, 3x3
 173 convolution layer + activation function (with batch normalization). Finally, an additional 1x1 convolution operation
 174 is applied to reduce the feature map to the required number of channels and generate the segmented image.

175 DenseNet121 transfer learning models were used for feature extraction and rock segmentation was performed with
 176 U-Net. Segmentation model was evaluated in terms of Intersection over Union (IoU) and f1-score metrics. For the
 177 calculate loss value dice loss was used. IoU, which is frequently preferred in segmentation problems, is also known as
 178 the Jaccard similarity coefficient (Jaccard, 1912). It is the ratio of correctly classified pixels to the sum of the number
 179 of pixels in that class and the predicted number of pixels. Mean IoU is the average IoU of all classes and presented in
 180 equation 1.

$$J(A, B) = \frac{|A \cap B|}{|A \cup B|} \quad (1)$$

181 The F1-Score is important in that it is not False Negative or False Positive, but a measurement metric that includes all
 182 error costs. It is the harmonic mean of Precision and Recall values (Equation 2).

$$F1\text{-Score} = \frac{2 \times \text{Precision} \times \text{Recall}}{\text{Precision} + \text{Recall}} \quad (2)$$

$$\text{Precision} = \frac{TP}{TP + FP}$$

$$\text{Recall} = \frac{TP}{TP + FN}$$

183 Where TP is True Positive, FP is False Positive and FN is False Negative.

184 3. Results

185 In this study, we created our own dataset. A large orthophoto image with a dimension of 2329x1587 was created
 186 from UAV images. This image needs to be patched for use in the segmentation model. A python script has been
 187 written for this purpose. It is possible to create the desired number and size of images with the written script. Random
 188 corner coordinates with the size of 256x256 patches were created. Obtaining images with the exact corner coordinates
 189 was prevented. Because of this condition, the program gives an error when too many images are wanted to be created.
 190 Also, the probability of creating very similar images increases. Using the grid method, 65 images can be obtained
 191 from the large orthophoto image. Using the random sampling method 600 images were obtained from the same image.

192 U-Net segmentation model was used with DenseNet121. IOU and F1 score values were used as metrics. Model

Table 1
Model parameters

Optimizer	Adam
Learning rate	0.0001
Batch size	8
Image size	256x256
Epoch	100

193 parameters were tested with different values. The parameters and values that provide the best results are given in the
194 table1 below.

195 IoU scores and losses graph of model is shown in Figure 6. The results of the model are satisfactory for the
196 segmentation task. Train IoU, validation IoU, train F1-score and validation F1-score were calculated as 0.8497%,
197 0.8461%, 0.9186%, and 0.9152%, respectively.

198 The trained model successfully detected rock blocks in the study area (Fig. 7). The boundaries of 3111 rocks of
199 various sizes were determined and created as a vector file (.shp). This method is not recommended for smaller areas.
200 Because sufficient training data cannot be created. In areas where there are several rock blocks, detection can also be
201 done manually. Sometimes there may be distortions at the edges and corners of the image. This causes errors in rock
202 block detection. Therefore, a larger area than the area where the rocks are located should be selected as the study area.

203 After the rocks were detected, each rock's volume and 3D surface area were calculated. These calculations were
204 performed using Python. Calculated values were saved in the shape file as fill volume, cut volume and 3D area.

205 In volume calculations, there must be a reference height or surface. In this study, the heights at the boundaries
206 of the rocks were selected as the reference height. The calculations were made using an image containing elevation
207 data. This image consists of pixels containing elevation values. These pixels form rows and columns. The elevation
208 values in each row were used to calculate the total volume. The polygons showing the boundaries of the rocks were
209 masked with elevation data. Thus, data with elevation values for each rock were obtained. Volumes were calculated
210 by proceeding along the rows. The slope was calculated by comparing the elevation values at the beginning and end
211 of the row. A new base elevation was determined for each pixel and the volumes were calculated from this elevation.

212 In this method, it is necessary to evaluate 3 different situations. In the first case, the first height and the last height
213 of the rows are equal. The starting elevation value is used as a reference height in this case. The volumes above this
214 height are calculated as the fill volume, and the below are calculated as the cut volume. In the second case, the first
215 height is greater than the last height of the rows. In the third case, the first height is less than the last height of the
216 rows. Different calculations must be made for each situation. These situations are shown in Figure 8.

217 Volume calculation can be easily done by multiplying the pixel area by the height. Heights need to be calculated
218 for each pixel. The starting and ending pixels along a row are assumed to be ground. These ground elevations are used

219 to find the slope, and each pixel's height is recalculated using this slope. Fill volume and cut volume were calculated
 220 using new heights and pixel areas. Slopes, fill volumes and cut volumes were determined using the method in Figure
 221 X. The total volumes (fill and cut) are found by summing the calculations made for each row.

222 The 3D Surface area was calculated by Python script. Calculations of flat surfaces can be found by multiplying
 223 pixel lengths. However, different methods must be used for irregular surfaces. The gradient method was used in 3D
 224 surface calculation. Height changes were calculated in X and Y directions, gradient vectors were obtained in each
 225 direction. Surface areas were calculated by using these vectors. The slope correction equation is used to determine the
 226 sloped surfaces (Equation 3).

$$\text{slope correction} = \sqrt{1 + \left(\frac{\partial z}{\partial x}\right)^2 + \left(\frac{\partial z}{\partial y}\right)^2} \quad (3)$$

$$\frac{\partial z}{\partial x} = \text{gradient in X direction}, \quad \frac{\partial z}{\partial y} = \text{gradient in Y direction}$$

The 3D surface area is calculated as following:

$$\text{3D surface area} = \text{pixel area} \times \text{slope correction}$$

227 4. Conclusions

228 This study aimed to segment rock blocks and calculate the volume and 3D surface areas of the blocks obtained as
 229 a result of segmentation. The methods used in the segmentation process provided the determination of the boundaries
 230 of rock blocks with high accuracy rates. In this way, the geometric properties of the blocks were analysed in detail.

231 U-NET deep learning network and DenseNet121 model were used as segmentation methods. The boundaries of
 232 rock blocks were determined accurately with the trained model.

233 The volume of each rock block was successfully calculated from the data obtained after segmentation. Similarly,
 234 the 3D surface areas of the blocks were calculated. High-resolution DEM data were used in volume and surface area
 235 calculations. Determination of block volumes and 3D surface areas is of critical importance, especially for rockfall
 236 simulations and engineering analyses. In addition, since the outputs of the study are coordinated vector data, they can
 237 be easily used in any GIS software. It can be a basis for different studies and analyses.

238 This study has presented a reliable method for segmentation and volume/surface area calculations and has also

239 directly contributed to engineering applications in terms of determining the physical properties of rock masses. The
240 segmentation section of the study is recommended for terrains containing a lot of rock blocks. It is possible to detect
241 rock blocks in a short time. In addition, this method can be used to automatically detect different types of terrain. Deep
242 learning models usually require a large amount of data for training. A large amount of data can be generated with the
243 Random Sampling method proposed in this study. Volume and 3D surface area algorithms can be used not only for
244 rock blocks but also for any object on the field. These algorithms only require precise DEM data and object boundaries.
245 For example, these calculations can be made for a single rock block. In these calculations, ground heights and object
246 heights must be determined clearly. When determining the object boundaries, they should be extended towards the
247 ground. If the boundaries only represent the object, the ground heights will not be considered, and the results will not
248 be correct. In some cases, the model can draw the boundaries of the rock blocks narrower. In this case, this problem
249 can be solved by adding buffers to the rock blocks.

250 As a result, this study provides a basis for volumetric and geometric analyses for rock mechanics, geology and
251 engineering applications, and can be expanded by testing on different rock types and fields in future studies.

252 **5. Acknowledgments**

253 The authors would like to acknowledge ...

254 **Code availability section**

255 Name of the code/library

256 Contact: e-mail and phone number

257 Hardware requirements: ...

258 Program language: ...

259 Software required: ...

260 Program size: ...

261 The source codes are available for downloading at the link: <https://github.com/...>262 **References**

- 263 Buslaev, A., Iglovikov, V.I., Khvedchenya, E., Parinov, A., Druzhinin, M., Kalinin, A.A., 2020. Albumentations: fast and flexible image augmentations. *Information* 11, 125.
- 264 Cao, Z., Liu, Z., Xu, G., Lin, H., Li, X., Nikitas, N., 2024. Risk assessment and prevention for typical railway bridge pier under rockfall impact, in: *Structures*, Elsevier. p. 106178.
- 265 Cruden, D.M., Varnes, D.J., 1996. Landslide types and processes. *Transportation Research Board, US National Academy of Sciences, Special Report* 247, 36–75.
- 266 Dunlop, H., 2006. Automatic rock detection and classification in natural scenes. Masters Thesis, Carnegie Mellon University .
- 267 Guo, Q., Wang, Y., Yang, S., Xiang, Z., 2022. A method of blasted rock image segmentation based on improved watershed algorithm. *Scientific Reports* 12, 7143.
- 268 Hutchinson, J., 1988. Morphological and geotechnical parameters of landslides in relation to geology and hydrogeology, landslides, in: *Proceedings of the fifth international symposium on landslides*, pp. 3–35.
- 269 Jaccard, P., 1912. The distribution of the flora in the alpine zone. 1. *New phytologist* 11, 37–50.
- 270 Ji, Z.M., Chen, T.L., Wu, F.Q., Li, Z.H., Niu, Q.H., Wang, K.Y., 2023. Assessment and prevention on the potential rockfall hazard of high-steep rock slope: a case study of zhongyuntai mountain in lianyungang, china. *Natural Hazards* 115, 2117–2139.
- 271 Kainthola, A., Pandey, V.H.R., Singh, P., Singh, T., 2023. Stability assessment of markundi hills using q-slope, smr and simulation tools, in: *Landslides: Detection, Prediction and Monitoring: Technological Developments*. Springer, pp. 87–107.
- 272 Karimpouli, S., Tahmasebi, P., 2019. Segmentation of digital rock images using deep convolutional autoencoder networks. *Computers & geosciences* 126, 142–150.
- 273 Keskin, İ., Polat, A., 2022. Kinematic analysis and rockfall assessment of rock slope at the unesco world heritage city (safranbolu/turkey). *Iranian Journal of Science and Technology, Transactions of Civil Engineering* 46, 367–384.
- 274 Kuang, B., Wisniewski, M., Rana, Z.A., Zhao, Y., 2021. Rock segmentation in the navigation vision of the planetary rovers. *Mathematics* 9, 3048.
- 275 Liu, W.l., Dong, J.x., Xu, H.h., Sui, S.g., Yang, R.x., Zhou, L.s., 2021. Trajectory analysis and risk evaluation of dangerous rock mass instability of an overhang slope, southwest of china. *Advances in civil engineering* 2021, 7153535.
- 276 Malladi, S.R.S., Ram, S., Rodríguez, J.J., 2014. Superpixels using morphology for rock image segmentation, in: *2014 Southwest Symposium on Image Analysis and Interpretation, IEEE*. pp. 145–148.
- 277 Ronneberger, O., Fischer, P., Brox, T., 2015. U-net: Convolutional networks for biomedical image segmentation, in: *Medical image computing and*

Short title

- 289 computer-assisted intervention–MICCAI 2015: 18th international conference, Munich, Germany, October 5-9, 2015, proceedings, part III 18,
290 Springer. pp. 234–241.
- 291 Song, Y., Shan, J., 2006. A framework for automated rock segmentation of the mars exploration rover imagery. URL: <https://api.semanticscholar.org/CorpusID:39798752>.
- 292
- 293 Varnes, D., 1978. Slope movement types and processes. *Landslides: analysis and control* .
- 294 Xue, Z., Chen, L., Liu, Z., Lin, F., Mao, W., 2021. Rock segmentation visual system for assisting driving in tbm construction. *Machine Vision and*
295 *Applications* 32, 77.
- 296 Yılmaz, H., Yılmaz, A., 2004. Divriği (sivas) yöresinin jeolojisi ve yapısal evrimi. *Türkiye Jeoloji Bülteni* 47, 13–46.

297 **List of Figures**

298	1	Location map	12
299	2	Geological map (1/25000 scale geological map of General Directorate of Mineral Research and Ex- 300 plorations) (a), rock blocks (b), settlement and rocks (c)	13
301	3	Workflow diagram	14
302	4	Train and test sampling areas. 1,5,9 test sampling area and 2,3,4,6,7,8 train sampling area	15
303	5	U-Net architecture	16
304	6	DenseNet121 IoU and Loss values	17
305	7	Result map of the model (a) original view, (b,c,d)zoomed views.	18
306	8	Volume calculation methods. (a) first height is greater than the last height of the rows,(b) b) first height 307 is less than the last height of the rows	19

Short title

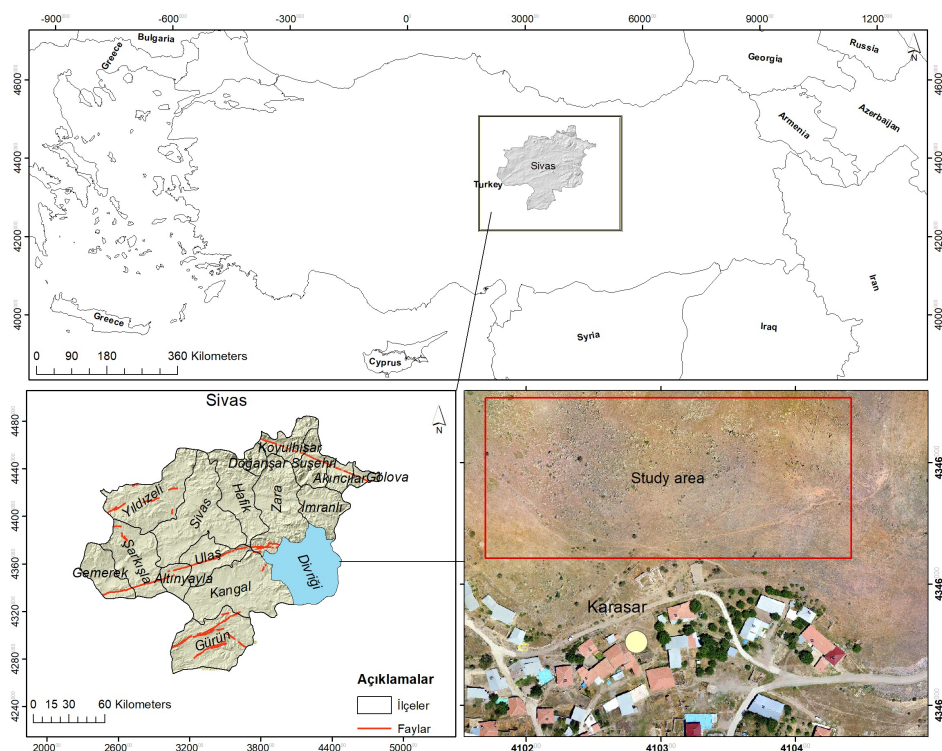


Figure 1: Location map

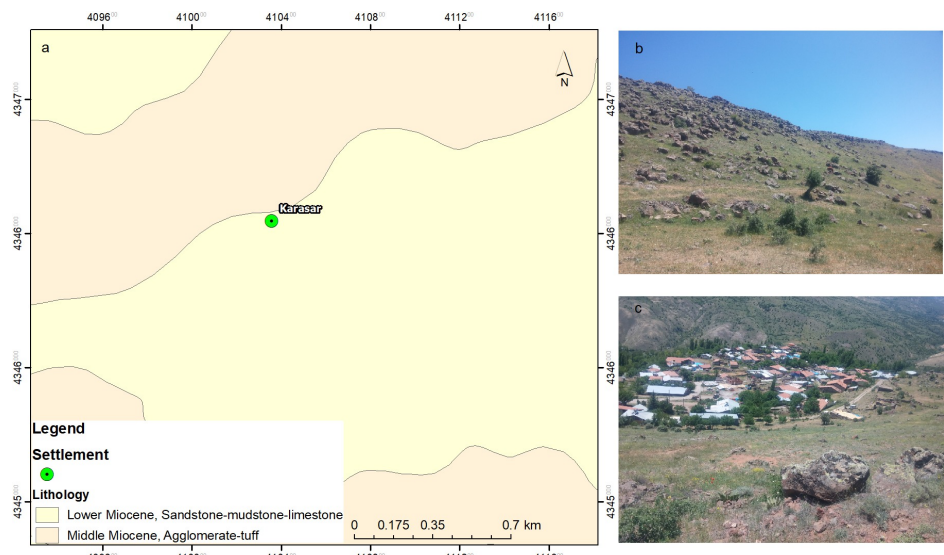


Figure 2: Geological map (1/25000 scale geological map of General Directorate of Mineral Research and Explorations (a), rock blocks (b), settlement and rocks (c)

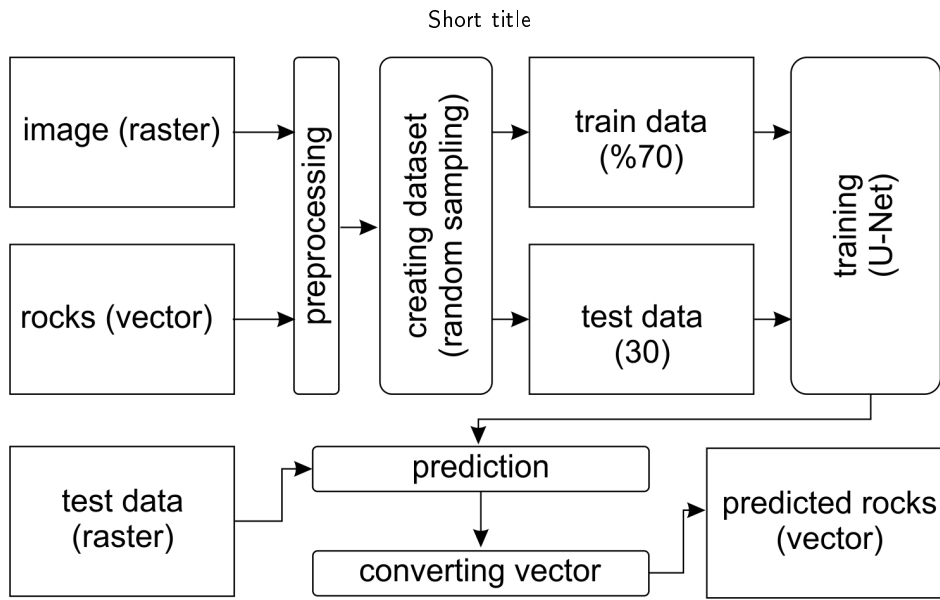


Figure 3: Workflow diagram



Figure 4: Train and test sampling areas. 1,5,9 test sampling area and 2,3,4,6,7,8 train sampling area

Short title

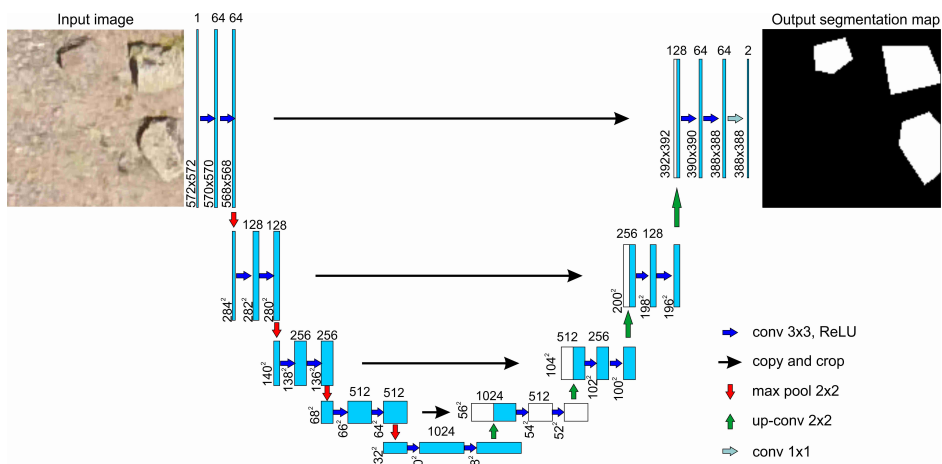


Figure 5: U-Net architecture

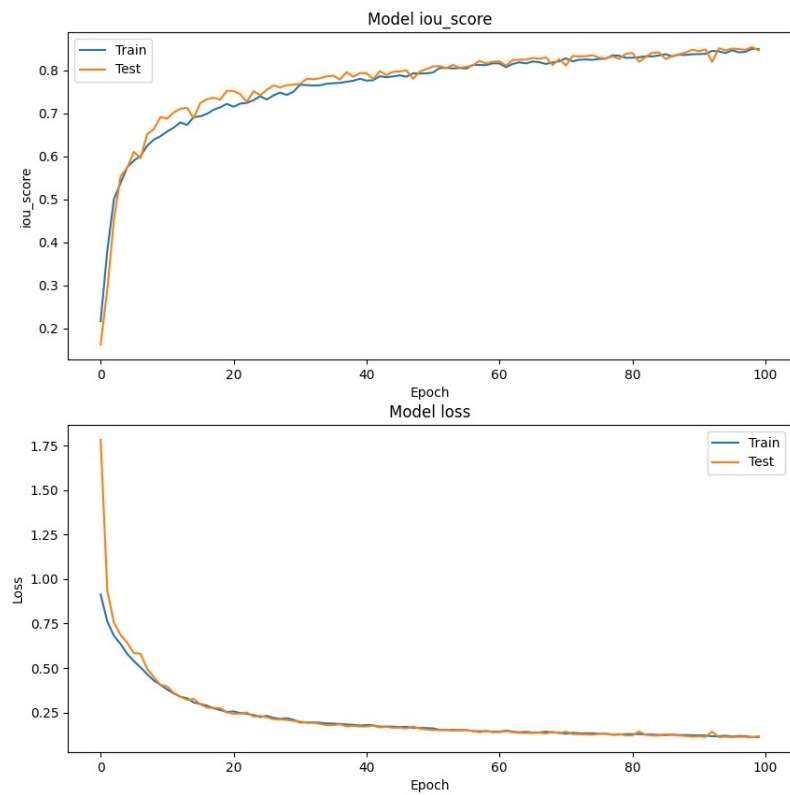


Figure 6: DenseNet121 IoU and Loss values

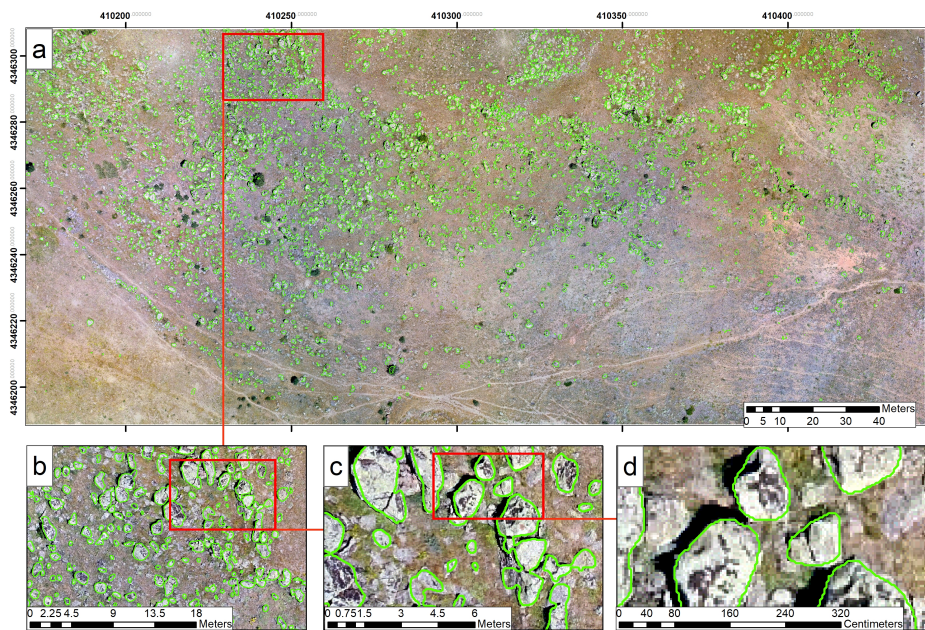


Figure 7: Result map of the model (a) original view, (b,c,d)zoomed views.

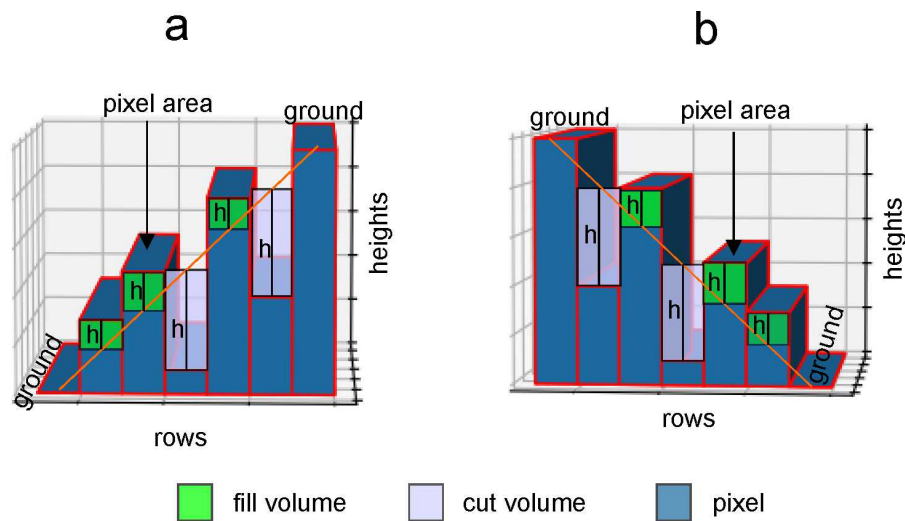


Figure 8: Volume calculation methods. (a) first height is greater than the last height of the rows,(b) b) first height is less than the last height of the rows